ACS Catalysis

Research Article

Cite This: ACS Catal. 2018, 8, 8879–8888

pubs.acs.org/acscatalysis

Identifying the True Catalyst in the Reduction of 4-Nitrophenol: A Case Study Showing the Effect of Leaching and Oxidative Etching Using Ag Catalysts

Eredzhep Menumerov,[†,§] Robert A. Hughes,[†,§] Spencer D. Golze,[†] Robert D. Neal,[†] Trevor B. Demille,[†] Justin C. Campanaro,[†] Kyle C. Kotesky,[†] Sergei Rouvimov,[∥] and Svetlana Neretina*[,†,‡]

[†]College of Engineering, University of Notre Dame, Notre Dame, Indiana 46556, United States

[‡]Department of Chemistry and Biochemistry, University of Notre Dame, Notre Dame, Indiana 46556, United States

[∥]Notre Dame Integrated Imaging Facility (NDIIF), University of Notre Dame, Notre Dame, Indiana 46556, United States

Supporting Information

ABSTRACT: The fundamental understanding of liquid-phase catalytic reactions is unavoidably complicated when the catalyst is prone to leaching since questions inevitably arise as to the true nature of the catalyst. While the catalytic reduction of 4-nitrophenol by borohydride is widely accepted as a trusted model reaction, it has faced little scrutiny concerning the potential impact of leached species or the appropriateness of assigning catalytic activity to the inserted nanostructures without rigorous experimental verification. Here, we present results from a spectroscopically monitored split test in which supported silver catalysts are physically separated from the reactants midway through the reaction. It is unambiguously demonstrated that the influence of leaching is far from benign, instead acting to extinguish the catalytic activity of the inserted nanostructures while giving rise to an unsupported heterogeneous catalyst that is the true catalytic entity. With only submonolayer quantities of silver leached from the supported structures, the unsupported species must be exceedingly catalytic. Moreover, it is shown that leaching is inherent to aqueous media containing dissolved oxygen, without which the supported nanostructures remain catalytically active. With the same nanomaterial being able to act either as a heterogeneous catalyst or as a reservoir from which leached metal is derived, such influences have undoubtedly compromised prior studies. We, nevertheless, capitalize on the sensitivity of 4-nitrophenol reduction to leached species by using it as a reaction-based indicator able to quantitatively determine the time dependence of the leaching process and enhancements to oxidative etching when silver, copper, palladium, platinum, and gold are exposed to chloride ions.

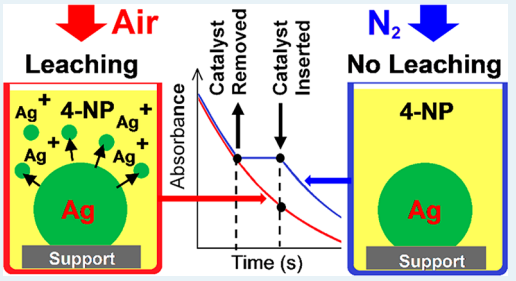

KEYWORDS: *leaching, oxidative etching, 4-nitrophenol, dissolved oxygen, split test, silver*

INTRODUCTION

The leaching of metal nanostructures in liquid-phase media is of central importance to heterogeneous catalysis.[1−4] It can lead to morphological disruptions that deactivate the catalyst, a decline in recycling performance, a loss of expensive precious metals, the contamination of the product, and the release of anthropogenic pollutants. From the perspective of catalyst design, the leaching process can be at odds with catalytic performance in that the most active sites are often those that are the most susceptible to leaching. This is especially true for catalytic reactions that are reliant on active sites characterized by surface steps and kinks[5] since less energy is required to remove atoms with low coordination. Strategies for stabilizing metal nanostructures against leaching include alloying with a metal offering greater chemical stability, their attachment to solid supports, and their confinement within a nano-reactor.[2,3,6−10] Noteworthy is that, while such remedies are regularly cited in the literature, their effectiveness in those same studies is often left unsubstantiated.

Obtaining a mechanistic understanding of the catalytic response derived from metal nanostructures is inescapably complicated by structures that are prone to leaching. In such a scenario, the true catalyst differs from that which was added to the solution. It also raises a concern as to whether the catalytic reaction is heterogeneous or homogeneous, i.e., does it occur on the surface of the nanostructure or does the nanostructure merely act as a reservoir from which catalytically active metal ions are derived. Such determinations can be difficult and highly contentious as is demonstrated by the intense debate that revolved around the use of Pd nanostructures in carbon−carbon coupling reactions (e.g., Suzuki−Miyaura and Heck

Received: June 14, 2018
Revised: August 10, 2018
Published: August 15, 2018

DOI: 10.1021/acscatal.8b02325
ACS Catal. 2018, 8, 8879−8888

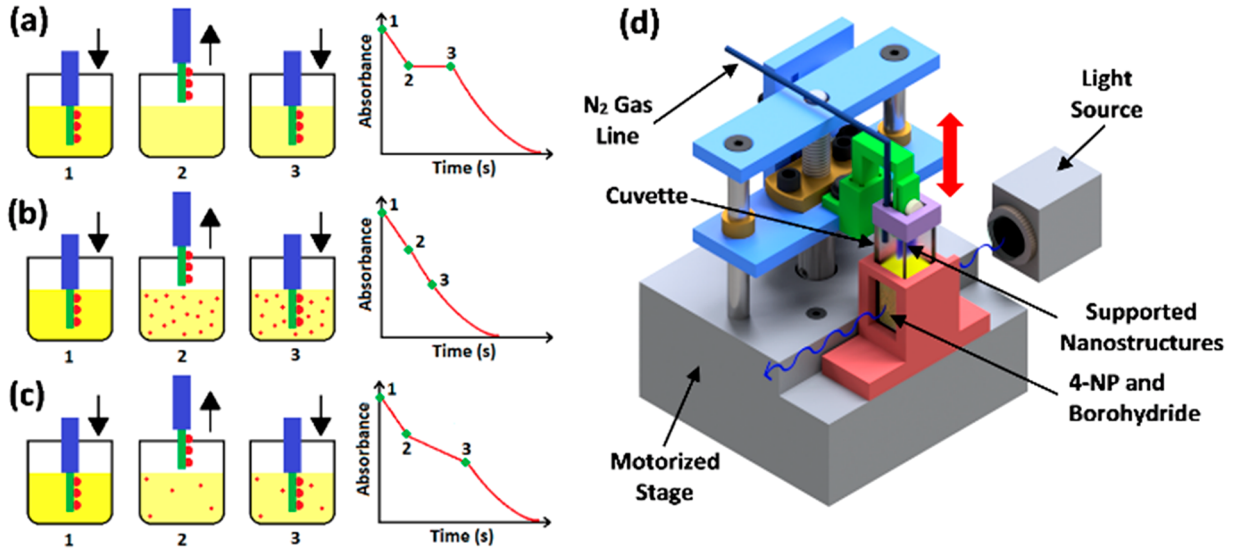

Figure 1. Schematics showing three possible scenarios for a spectroscopically monitored split test for the reduction of 4-NP by borohydride in which the catalytic turnover is due to (a) a supported heterogeneous catalyst, (b) an unsupported heterogeneous catalyst derived from leached species, and (c) a combination of the unsupported and supported heterogeneous catalysts. (d) Schematic of the custom-built motorized stage used to raise and lower supported nanostructures from a reactant-filled cuvette while spectroscopically monitoring the outcome.

reactions).[4,11−14] In certain instances, it is also possible for leached ions to be reduced back to neutral species. Such species can then reconfigure the original nanostructure through redeposition and Ostwald ripening[2] or form a population of smaller nanoparticles[15−17] that could, in fact, become the true heterogeneous catalyst. Making such determinations can be an arduous task that is reliant on analytical techniques capable of determining the extent of the leaching process as well as *in situ* and *ex situ* characterization of the catalysts.[4,11−14,18−20] Procedures have also been devised to identify the true catalyst including selective poisons, three phase tests, consistent yield tests, and hot filtration tests,[4,21−23] the latter of which is a form of split test in which the reaction is monitored after the heterogeneous component has been physically separated from any leached species.

The reduction of 4-nitrophenol (4-NP) by borohydride is widely recognized as a trusted model reaction for assessing the catalytic activity of nanostructures in an aqueous solution.[24−26] The reaction, which only occurs if a catalyst is present, allows for real-time spectroscopic monitoring from which precise kinetic parameters are readily obtained. There is little debate as to whether the reaction is homogeneous or heterogeneous, as it is almost universally accepted that it, along with other hydrogenation reactions, occurs on the surface of the catalyst.[20,24−29] As such, most studies simply assert that the nanostructure added to the reaction is the true catalyst without experimental verification. With such an assertion comes the underlying assumption that nanostructure leaching has little to no impact on catalytic activity and that leached species have no influence on reaction kinetics. Several studies, however, have argued that leaching can play a significant role in the catalytic reduction of 4-NP. Zhang and Xu,[7] for example, demonstrated that Pd nanoparticles confined within a CeO_2 hollow core were far more resistant to leaching than identical Pd nanoparticles supported on the surface of a solid CeO_2 sphere. The leached nanoparticles underperformed their leach-resistant counterparts in terms of both catalytic turnover and recyclability. It was concluded that leaching resulted in the deactivation of the Pd catalyst. Katz and co-workers[17] carried out poisoning experiments that led to the conclusion that the true catalyst was not the added Au nanoparticles but a highly catalytic leached species present in exceedingly small quantities. They, however, provided no direct evidence that such a species existed.

Recently, we demonstrated the catalytic reduction of 4-NP by borohydride through the direct injection of aqueous Au^{3+}, Ag^{+}, Pd^{2+}, and Cu^{2+} ions.[30] This differs from the vast majority of the literature in that the reaction is not reliant on the injection of preformed catalysts. Instead, heterogeneous catalysis occurs on nanostructures that were formed near-instantaneously due to the reduction of the injected metal ions by borohydride. This one-step process resulted in impressive catalytic activity, yielding turnover frequencies as high as 65 000 h^{-1} at 0.1 mol %. Recognizing that ions leached from preformed catalysts could, in an analogous manner, form smaller nanostructures with exceedingly high turnover frequencies, we forwarded the possibility that leach-prone nanostructures give rise to the formation of a second catalytically active species and, in doing so, compromise the benchmarking of catalysts using this model reaction. Here, using a spectroscopically monitored split test in which a supported Ag catalyst is controllably inserted and retracted from a reactant-filled cuvette, it is unambiguously demonstrated that leaching not only acts to deactivate the inserted catalyst but leads to the rapid formation of an unsupported heterogeneous catalyst that is far more active. Moreover, it is shown that the leaching process is entirely dependent on the presence of dissolved oxygen within the aqueous solution, without which the catalyst surface remains intact and active. The study also demonstrates the utility of the devised split test as a straightforward and inexpensive optical diagnostic able to identify the true catalyst and detect leached species with submonolayer sensitivity.

RESULTS

Spectroscopically Monitored Split Test. The catalytic reduction of 4-NP by borohydride lends itself to spectroscopic monitoring since both it and the product, 4-aminophenol (4-

DOI: 10.1021/acscatal.8b02325
ACS Catal. 2018, 8, 8879−8888

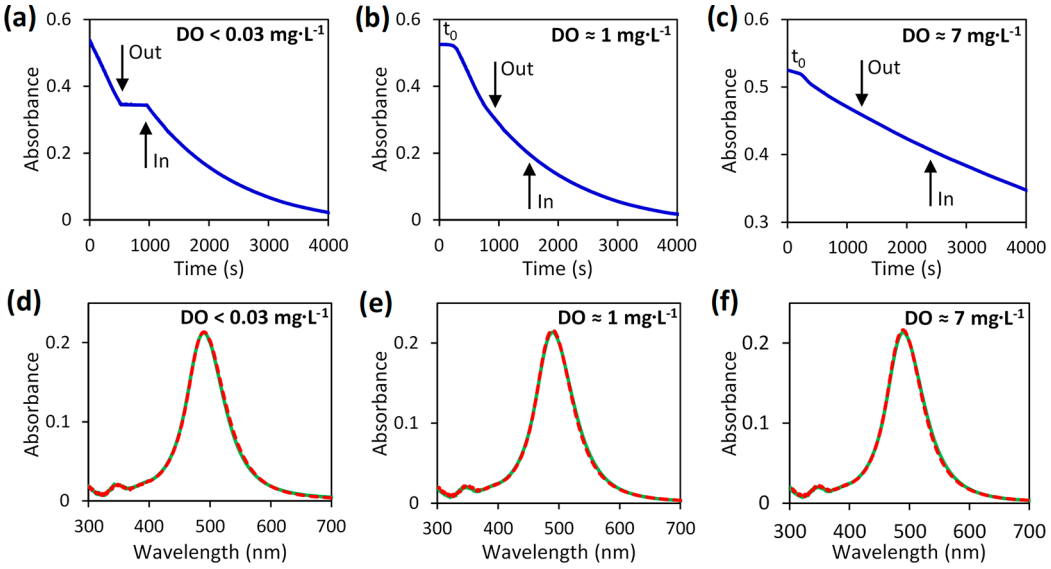

Figure 2. Time dependence of the 400 nm 4-NP absorbance as the supported Ag nanostructures undergo the split test for reactants having a dissolved oxygen concentration of (a) <0.03, (b) 1, and (c) 7 mg·L^{-1}. (d–f) Absorbance spectra of the supported nanostructures taken before (green) and after (red) the reaction for the same three dissolved oxygen concentrations.

AP), exhibit prominent absorptions at 400 and 300 nm, respectively. By monitoring the time-dependent decrease in the 400 nm absorption, an apparent reaction rate constant, k_{app}, is readily extracted from the slope of the $\ln(A/A_0)$ vs time plot, where A/A_0 is the 4-NP absorbance normalized to its value at the onset of the reaction.[26] Of significance to the current study is the pronounced effect that dissolved oxygen has on the reaction in that it leads to diminished catalytic activity[30] and the establishment of an induction period after catalyst insertion[31] during which the absorbance is near-constant. Its influence is further complicated by the fact that borohydride acts as a slow scavenger of dissolved oxygen whose effectiveness is enhanced in the presence of a catalyst and lessened when the reaction is carried out under air due to the continuous uptake of O_2 into the aqueous solution.[31] Such influences give rise to varying results depending on (i) the sequence and timing in which the reactants are combined, (ii) whether an inert gas is used to purge some or all of the reactants, and (iii) whether the reaction is carried out under the protection of an inert gas.[31]

With the aforementioned constraints in mind, a spectroscopically monitored split test was devised that is capable of determining whether leached species contribute to the catalytic reduction of 4-NP in both the presence and absence of dissolved oxygen. It is reliant on a dip catalyst modality[32−34] where the reaction is initiated by dipping supported nanostructures into a reactant-filled cuvette followed by their removal when the reaction is complete. In the devised test, the catalyst is inserted into the reactants at t = 0 s, removed midway through the reaction, and then reinserted before the reaction ends. By physically separating the catalyst from any unsupported catalysts formed through leaching and precipitation, it is possible to identify the true catalytic entities by monitoring the 400 nm 4-NP absorbance. Figure 1a−c presents schematic representations for three possible scenarios. In the first scenario, where the supported catalyst is leach-resistant, the reaction begins when the catalyst is inserted, is halted when it is removed, and then continues upon reinsertion (Figure 1a). In the second scenario, the supported nanostructure has negligible catalytic activity but is prone to leaching that leads to the rapid formation of an unsupported catalyst. In this case, the reaction begins when the supported nanostructures are inserted, continues at the same rate when they are removed, and is insensitive to their reinsertion (Figure 1b). In the third scenario, where the nanostructures leach but remain catalytically active, the reaction begins when the nanostructures are inserted, continues at a slower rate when removed, and then speeds up upon reinsertion (Figure 1c).

The split test was made possible by retrofitting the sample compartment of a Jasco V−730 spectrophotometer with a motorized stage designed to lower and raise supported nanostructures into and out of reactants contained within a 1 cm path length cuvette (Figure 1d). When inserted, the supported nanostructures were at a level that in no way obstructed the spectroscopic probe beam. The stage was also equipped with a gas line that continuously flowed N_2 over the reactants to prevent the uptake of dissolved oxygen. A detailed description and an image of the stage are provided as Figure S1. It is noted that, by design, the tests were performed using an exceedingly small amount of catalyst (≈2.2 μg) so as to prolong the duration of the reactions to timespans that facilitated a workable insertion−removal−reinsertion procedure.

Split Test Results. Solid-state dewetting[35] was used to self-assemble supported Ag nanostructures on sapphire substrates by sputter depositing ultrathin films at room temperature followed by a heating procedure. The structures produced had an average diameter of 33 nm (Figure S2). Nanostructures produced in this manner do not have any capping or stabilizing agents which, hence, removes the possibility of any ligand interference in both the leaching and catalytic processes. Figure 2a−c shows the split test results for three identical supported catalysts where the dissolved oxygen concentration of the reactants at t = 0 s was varied from less than 0.03 to 7 mg·L^{-1} by either purging the solution with N_2 gas[31] or allowing borohydride the time needed to scavenge the dissolved oxygen to the required level. For the lowest dissolved oxygen concentration, the split test shows the response expected for

DOI: 10.1021/acscatal.8b02325
ACS Catal. 2018, 8, 8879−8888

a reaction driven by a supported heterogeneous catalyst (Figure 2a). This result is in stark contrast to that observed when the dissolved oxygen concentration is at 1 mg·L^{-1}, which shows the response expected for a reaction that is solely driven by an unsupported species derived from leached metal (Figure 2b). For these two cases, the reaction rate is nearly identical. When the oxygen content is increased to 7 mg·L^{-1}, the response, once again, shows the behavior expected for a reaction entirely driven by an unsupported species (Figure 2c). For this case, the reaction is slowed considerably due to the deleterious effects that dissolved oxygen has on k_{app}.[30] For all three cases, the supported structures show nearly identical plasmon resonances before and after the reaction (Figure 2d–f). As expected, an induction period (t_o) is observed for the two cases where dissolved oxygen is present in quantities of significance.[31] It should be noted that all of these results are highly reproducible. Furthermore, they are not unique to dewetted Ag nanostructures since solution-deposited and galvanically replaced Ag both show the same response (Figures S3 and S4).

The implications of the results presented in Figure 2 are numerous. First, they provide unambiguous evidence for the formation of an unsupported active species. Second, the active species is highly catalytic. The fact that the plasmon resonance of the supported Ag nanostructures shows no discernible change over the course of the reaction (Figure 2e,f) indicates that only a small quantity of Ag has been leached, yet the reaction rate derived from this leached material is nearly identical to that obtained for all of the supported structures in the absence of leaching (Figure 2a). Third, the leaching process is entirely dependent on the presence of dissolved oxygen within the aqueous reactants. While it is not surprising that leaching has its origins in oxidative etching,[36,37] it implies that the leaching process will be turned off as borohydride scavenges dissolved oxygen, the ramification of which is that leaching can recommence if the nanostructures are exposed to fresh reactants containing dissolved oxygen (*vide infra*). Moreover, the lack of leaching in the absence of dissolved oxygen indicates that neither borohydride nor 4-NP leach Ag. Fourth, supported Ag nanostructures can act either as heterogeneous catalysts or as reservoirs of leached species from which the true catalyst is derived. This has inevitably led to nanostructures being labeled as highly catalytic when they are, in fact, merely prone to leaching. From the standpoint of using the reduction of 4-NP by borohydride as a model reaction for benchmarking the catalytic response of nanostructures, such test results represent what are, in essence, false positives. Fifth, the catalytic sites on the supported Ag nanostructures are those that are most prone to leaching. The fact that no response is observed when leached supported structures are removed and then reinserted into the reactants (Figure 2b,c) provides a clear indication that the supported nanostructures have been rendered catalytically inactive. Further confirmation that catalytic activity is lost is provided in Figure S5. Such a result is not surprising if the catalytic sites are those with low coordination since they are also prone to leaching.

Quantification of the Fraction of Leached Material. The split test results presented in Figure 2b,c indicate that a small, but unknown, fraction of Ag leaches from the supported nanostructures when exposed to dissolved oxygen. The fact that there is no discernible blue shift in the localized surface plasmon resonance (LSPR) of the supported nanostructures (Figure 2e,f) resulting from a loss in diameter due to the leaching event suggests that only a small amount of Ag is lost. Discrete dipole approximation (DDA) simulations[38] were carried out in an effort to quantify the amount of material that could leach from a nanostructure and remain undetectable. Figure 3a shows a schematic of the simulated nanostructure

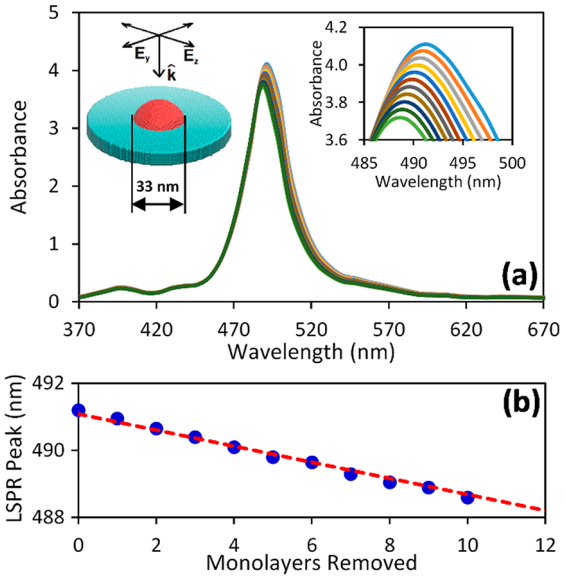

Figure 3. (a) DDA simulations of the blue shift in the LSPR peak for the nanostructure shown schematically in the upper left inset as its diameter is reduced by 10 monolayers in 1 monolayer increments. The top right inset shows an expanded view of the LSPR peak. (b) Dependence of the LSPR peak position as a function of the number of monolayers removed.

and the absorbance spectra as 1 to 10 monolayers are removed. A plot of the LSPR peak position as a function of the number of monolayers removed is shown in Figure 3b. If, from an experimental standpoint, it is possible to reliably detect a 0.5 nm LSPR blue shift, then these simulations indicate that 2 monolayers would have to be lost to leaching for detection to occur. The simulations indicate that the absolute value of absorbance could prove more sensitive, but reproducibility in sample positioning within the spectrometer's sample holder makes this parameter less reliable than the simulations would suggest. It should also be recognized that the spectroscopic signature of leaching is likely to be more apparent if it gives rise to a shape change.

If the leached material enters the solution as Ag^+, then unsupported heterogeneous catalysts can form since borohydride is a reducing agent.[30,39,40] If Ag^+ ions derived from aqueous $AgNO_3$ behave identically to those that are leached, then it should also prove possible to spectroscopically determine the quantity of leached material by injecting known quantities of Ag^+ into identical solutions of 4-NP and borohydride to determine the concentration that gives rise to the same catalytic activity. Figure 4a shows a schematic of the experimental procedure used to determine the quantity of material leached from supported Ag catalysts exposed to reactants with initial dissolved oxygen concentrations of 1 and 7 mg·L^{-1}. It begins by injecting 0.1 mL of a known molarity of aqueous $AgNO_3$ into a 1.9 mL solution of 4-NP and borohydride with the desired dissolved oxygen concentration. The Ag^+ ions are then reduced to form nanostructures that act

DOI: 10.1021/acscatal.8b02325
ACS Catal. 2018, 8, 8879–8888

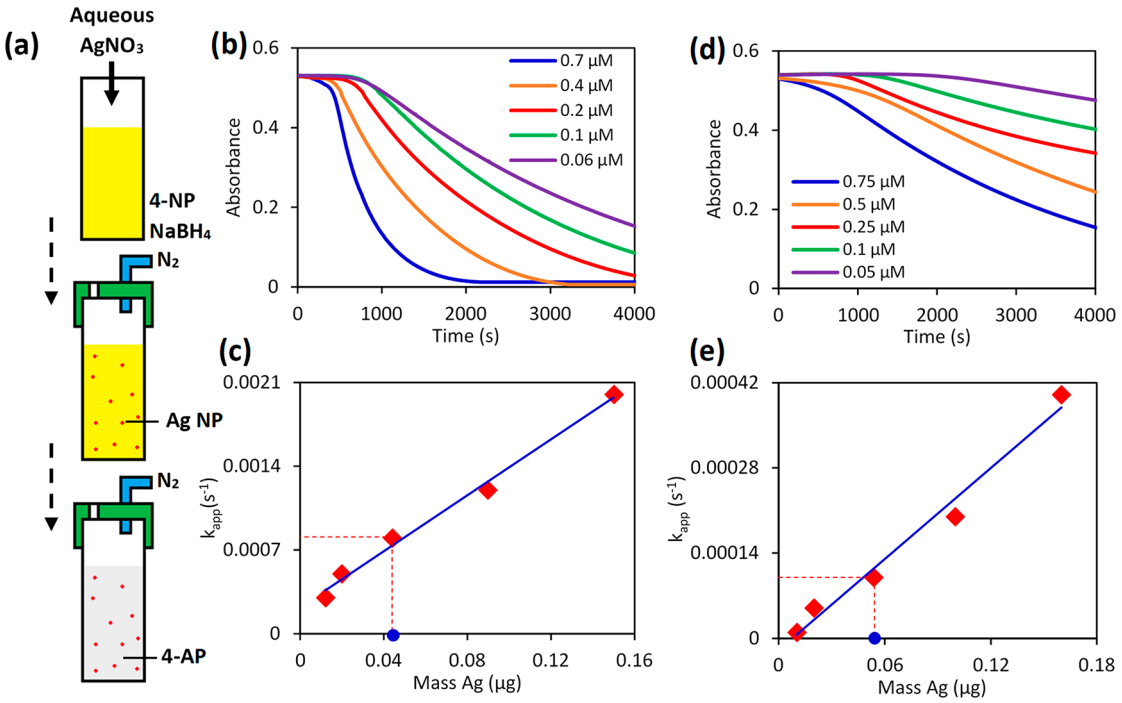

Figure 4. (a) Schematic showing the procedure used to generate calibration curves for determining the quantity of Ag leached from the supported nanostructures during split tests. The time-dependent absorbance and calibration curve for reactants with dissolved oxygen concentrations of (b, c) 1 and (d, e) 7 mg·L^{-1}. Also shown on the calibration curves are dashed lines connecting the k_{app} value obtained from the split test (blue dot) to the predicted mass of leached Ag.

as heterogeneous catalysts capable of transforming 4-NP into 4-AP. By spectroscopically monitoring such reactions, it is possible to determine the dependence of k_{app} on the Ag^+ concentration and, in doing so, generate a calibration curve from which the quantity of leached material can be extracted.

Figure 4b,c shows the time-dependent absorbance data for various Ag^+ concentrations and the resulting calibration curves for the 1 mg·L^{-1} dissolved oxygen concentration. Using the value of k_{app} extracted from the split test results (Figure 2b) in combination with the calibration curve reveals that 0.043 μg of Ag leached from the supported nanostructures (dashed lines in Figure 4c), which corresponds to a 2 mL solution with an Ag^+ concentration of 0.2 μM. The supported nanostructures, which had an initial mass of 2.2 μg, hence, lost 2% of their mass. Figure 4d,e shows the corresponding time-dependent absorbance and calibration curve for the 7 mg·L^{-1} dissolved oxygen concentration. Using the k_{app} value derived from Figure 2c reveals that this supported catalyst lost 0.054 μg of Ag to leaching or 2.5% of its mass. For this case, the solution has an Ag^+ concentration of 0.25 μM. Given that these near-hemispherical supported Ag nanostructures have an average diameter of 33 nm, mass losses of 2% and 2.5% both represent submonolayer quantities (≈4% of the mass is contained within the first monolayer), a result consistent with the aforementioned DDA calculations. In an effort to further validate this method for spectroscopically quantifying the amount of leached material, inductively coupled plasma optical emission spectrometry (ICP−OES) was carried out on the product of the reaction. The measurements revealed an Ag mass loss to leaching of 0.048 and 0.056 μg for the 1 and 7 mg·L^{-1} dissolved oxygen concentrations, values that are in good agreement with 0.043 and 0.054 μg values obtained from the spectroscopic measurements. The demonstrated procedure, therefore, provides a straightforward and inexpensive means to spectroscopically determine the quantity of leached material with submonolayer sensitivity.

TEM Characterization of the Unsupported Ag Nanostructures. While the split test is able to identify the existence of an unsupported active species, it is unable to discern whether it is a homogeneous or heterogeneous catalyst. Studies involving the direct injection of solvated ions into 4-NP and borohydride have demonstrated the formation of colloidal nanostructures.[30,39,40] If leached ions behave in a similar manner, then the nanostructures formed should be detectable. To this end, the product of a split test, where the initial dissolved oxygen concentration was set to 1 mg·L^{-1}, was dropcast onto a TEM grid and examined. Figure 5a,b shows TEM images that reveal the existence of unsupported Ag

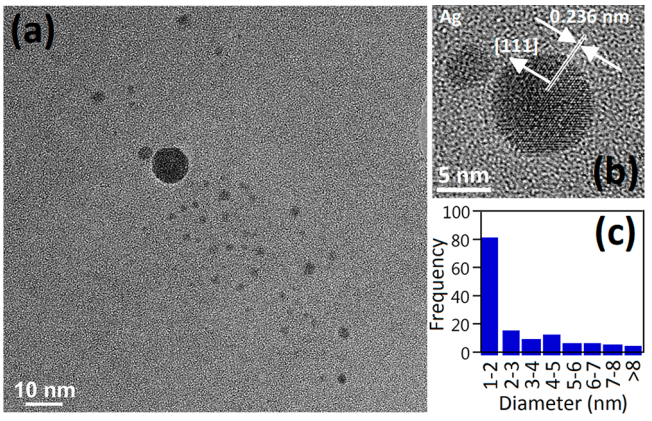

Figure 5. (a, b) TEM images of the unsupported heterogeneous catalysts derived from the Ag leached from the supported catalysts and (c) their associated size distribution.

DOI: 10.1021/acscatal.8b02325
ACS Catal. 2018, 8, 8879−8888

nanostructures. The vast majority of these structures are spherical in shape with diameters that are less than 3 nm (Figure 5c). The observation of these structures supports our claim that the unsupported active species forms through a process whereby Ag^+ first leaches from the supported catalyst due to oxidative etching and is then reduced by borohydride to form a population of colloidal Ag nanostructures that act as highly active heterogeneous catalysts. Also of note is that nanostructures prepared through the direct injection of aqueous $AgNO_3$ into 4-NP and borohydride result in the formation of Ag nanostructures that appear quite similar to those formed from leached species (Figure S6), a result that further validates our assumption that the leached and injected species behave similarly.

Catalytic Reduction of 4-NP as a Reaction-Based Indicator of Oxidative Etching. With the catalytic reduction of 4-NP being highly sensitive to small quantities of leached material, there exists the opportunity to use this reaction as a simple and inexpensive probe of the leaching process. In this section, two proof-of-principle demonstrations are presented that characterize (i) the time dependence of leaching from supported Ag nanostructures and (ii) enhancements to oxidative etching that occur when various noble metals are exposed to saline solutions. For both cases, the catalytic reduction of 4-NP is used as a reaction-based indicator for leached metal.

Time-Dependent Leaching from Supported Ag Nanostructures. The supported Ag nanostructures used in the split test can undergo oxidative etching until the dissolved oxygen is scavenged by borohydride. There is, therefore, the possibility for continued leaching to occur when these same structures are exposed to fresh reactants containing dissolved oxygen. Figure 6a shows a schematic of the procedure used to quantify the time-dependent leaching from supported Ag nanostructures when exposed to water with a dissolved oxygen concentration of 8.3 $mg{\cdot}L^{-1}$ (i.e., the ambient value). For this case, there is no reason for the leaching process to cease since the surface of the water is exposed to air and the borohydride scavenger is absent. The procedure begins by placing the supported catalysts in a cuvette containing 1 mL of water for a set time interval. The catalyst is then removed and the water containing leached Ag is purged with N_2 gas. The solution is then poured into a cuvette containing a purged solution of 4-NP and borohydride, and the ensuing reaction is monitored. This procedure was repeated for six identical samples for time intervals extending from 0.5 to 20 min. The quantity of leached Ag was then derived from a calibration curve (Figure S7) obtained using known quantities of aqueous $AgNO_3$ subjected to the same N_2 purge and 4-NP reaction. The results, presented in Figure 6b (red diamonds), show the mass lost to leaching from supported Ag nanostructures as a function of the time exposed to dissolved oxygen. These results are in good agreement with those obtained using ICP−OES (blue dots) performed on identically prepared samples. When carrying out such experiments, it is imperative that the dissolved oxygen be completely removed as even structures formed through the leaching process lose catalytic activity when exposed to dissolved oxygen.

The data presented in Figure 6b indicates that the rate of nanostructure leaching diminishes over time where little change is observed after 15 min. Such behavior likely stems from the loss of Ag from low coordination sites, which over time leaves behind a more ordered and stable surface that

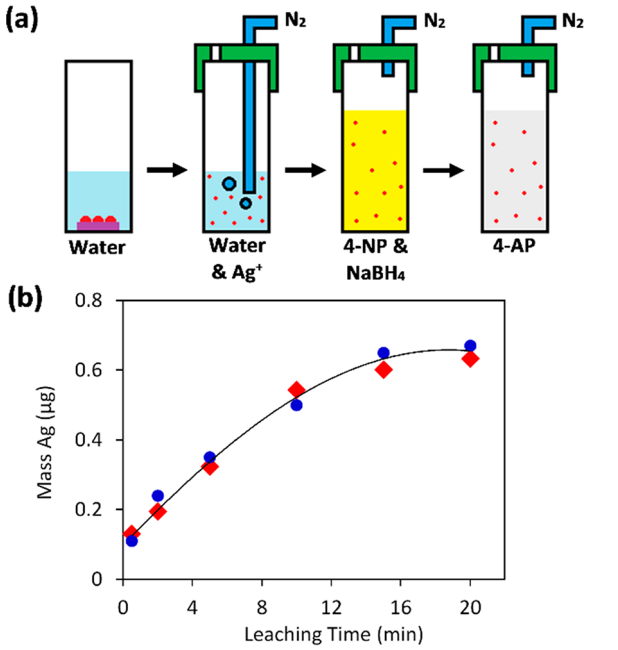

Figure 6. (a) Schematic showing the procedure used to determine the amount of Ag leached from supported nanostructures where the reduction of 4-NP is used as a reaction-based indicator. (b) Mass loss from supported Ag nanostructures as a function of time exposed to water with a dissolved oxygen concentration of 8.3 $mg{\cdot}L^{-1}$ as obtained from spectroscopic (red diamonds) and ICP−OES measurements (blue dots). The black curve is a guide for the eye.

becomes increasingly resistant to leaching. Briggs et al.[19] came to a similar conclusion when monitoring the leaching characteristics of Pd nanostructures using extended X-ray absorption fine structure spectroscopy (EXAFS) in combination with small angle X-ray scattering (SAXS). What is striking about this data is that the quantity of leached Ag is 13× that which was leached during the split test shown in Figure 2b. The implication of this result is that supported Ag catalysts could be cycled through numerous reactions where, in each case, the catalytic response is derived from an unsupported leached species. A small number of recycling tests, therefore, do not provide unambiguous evidence for supported nanostructures being labeled as the true catalyst.

Metal Leaching in Saline Solutions. Noble metal nanostructure synthesis has often employed oxidative etching as a means to manipulate growth modes.[36,37] Such routes typically accelerate these corrosive processes through the addition of halide ions. In an effort to quantify this enhancement to leaching, films of Ag, Cu, Pd, Pt, and Au were subjected to the same procedure as shown in Figure 6a using room temperature aqueous solutions with a (i) dissolved oxygen concentration of 8.3 $mg{\cdot}L^{-1}$ and (ii) an identical solution to which 15 μM NaCl is added. Figure 7 shows a histogram of the k_{app} values obtained for each metal in the presence and absence of Cl^- ions. The sensitivity of Ag, Cu, and Pd to leaching in the presence of Cl^- is consistent with the literature.[41−43] It is also not surprising that the more noble metals (i.e., Au and Pt) show greater resistance to leaching. While the observed enhancements are inevitably dependent on the Cl^- concentration and water temperature, this initial demonstration provides an indication that such experiments could provide valuable insights into oxidative etching when carried out in the presence of halide ions. With Cu and Pd

DOI: 10.1021/acscatal.8b02325
ACS Catal. 2018, 8, 8879−8888

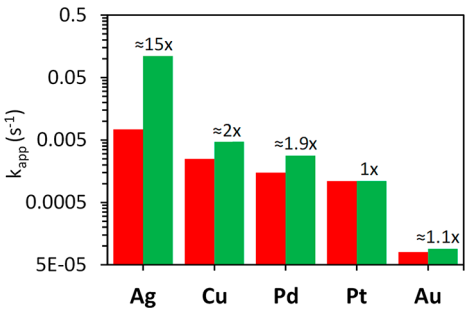

Figure 7. Histogram showing the values of k_{app} obtained for catalytic nanostructures reduced from leached metal derived from films of Ag, Cu, Pd, Pt, and Au that have undergone oxidative etching (red) and oxidative etching in a 15 μM NaCl solution (green). The enhancement to k_{app} due to the presence of Cl^- ions is shown for each metal.

films showing significant leaching that gives rise to the formation of unsupported catalysts in 4-NP reduction, it raises the concern that supported nanostructures of these metals will behave similarly and, in doing so, compromise the conclusions drawn when using 4-NP reduction as a model reaction. The fact that Au and Pt films show a resistance to leaching suggests that the 4-NP literature related to these metals is far less prone to the effects described herein.

DISCUSSION

While the catalytic reduction of 4-NP is often viewed as a trusted model reaction for assessing heterogeneous catalysts, the current study indicates that further scrutiny is warranted when interpreting its results. It is particularly troubling that identical nanostructures can act as either heterogeneous catalysts or catalytically inert reservoirs of leached ions from which the true heterogeneous catalyst is derived. Having identified dissolved oxygen as the cause of leaching, it becomes possible to rid this model reaction of such complications. To achieve this, the reactants, as well as any catalyst-containing solutions, must be efficiently purged of dissolved oxygen and the reaction must be carried out under an inert gas. The presence or absence of an induction period can, to a large extent, provide a measure of the efficacy of such procedures since it is absent when the dissolved oxygen is removed.[31] Its presence, however, raises the concern that some or all of any observed catalytic activity originates from leached material, a concern that is heightened if halide ions, which are often released from metal precursors in nanostructures synthesis,[37] enter the reaction. At the same time, it should not be assumed that all nanostructures leach since particular facets or surface ligands could act to stabilize the surface against leaching.

The sensitivity of the catalytic reduction of 4-NP to leaching not only identifies potential pitfalls in its use as a model reaction but also presents opportunities for using this reaction as a straightforward and inexpensive optical diagnostic for quantitatively assessing the oxidative etching of supported nanostructures. Demonstrated in the current study is the ability to detect leached species with submonolayer sensitivities, map out the time dependence of the leaching process, and characterize enhancements to the leaching rate due to the presence of Cl^- ions. Such findings further the understanding of nanostructure stability in aqueous environments, a topic of relevance not just to catalysis but also to nanostructure synthesis,[36,37,44,45] the preparation of pharmaceuticals,[46,47] wastewater management,[48,49] and the use of Ag nanostructures as antimicrobial agents.[50−53] The potential, therefore, exists to extend the use of the tests presented in this study to assess (i) the catalytic durability of nanostructures presenting various facets, surface ligands, compositions, and defect structures, (ii) leaching mitigation strategies involving the use of alloys, nanoreactors, and host frameworks, (iii) the leaching strength of various chemical, photoactive, and thermal environments, and (iv) the effectiveness of metal and oxygen scavengers.

CONCLUSION

In summary, we have provided incontrovertible evidence that Ag leached from supported catalysts leads to the formation of unsupported heterogeneous catalysts with exceedingly high catalytic activity toward the reduction of 4-NP by borohydride. The implication of this finding is that nanostructures, when introduced into this model reaction, may appear as excellent heterogeneous catalysts when they are, in fact, merely prone to leaching. By identifying dissolved oxygen as being central to the leaching process, it becomes possible to rid the reaction of these leached species by purging the reactants with N_2 gas, but where prudence must be exercised since as little as 1 mg·L^{-1} of dissolved oxygen is shown to be highly problematic for the case of Ag. In addition, it is shown that it is possible to experimentally mimic the response of leached Ag using Ag^+ ions derived from $AgNO_3$ and, in doing so, provide an effective means for estimating the quantity of leached material with submonolayer sensitivities. Such a demonstration opens up the possibility of using the catalytic reduction of 4-NP as a simple and inexpensive reaction-based indicator for elucidating the mechanism governing oxidative etching, identifying leach-resistant catalysts, and further advancing oxidative etching as a versatile tool in the synthesis of complex nanostructures.

EXPERIMENTAL SECTION

Chemicals and Materials. Sputter deposition targets of Ag, Au, Cu, Pt, and Pd were cut from 0.5 mm thick foils with purities of 99.9985%, 99.9985%, 99.9999%, 99.99%, and 99.95+%, respectively (Alfa Aesar). The supported Ag nanostructures were formed on [0001]-oriented sapphire substrates (7 mm × 12 mm × 0.5 mm) that were cleaved from 3 in. wafers (MTI Corp.). The thin film work utilized soda-lime glass substrates (12 mm × 12 mm × 1 mm). Solutions for catalysis were prepared using 4-NP (Fluka), $NaBH_4$ (Fluka), and DI water with a resistivity of 18.2 MΩ cm^{-1}. The solution-based overgrowth of Ag nanoparticles utilized silver nitrate ($AgNO_3$, Sigma-Aldrich) and L-ascorbic acid (AA, Sigma-Aldrich). Galvanic replacement reactions utilized hydrogen tetrachloroaurate(III) trihydrate ($HAuCl_4 \cdot 3H_2O$, Sigma-Aldrich). Ultrahigh purity Ar and N_2 gases (Airgas) were used as an inert background for dewetting Ag films and to purge the reactants in catalysis experiments, respectively. All chemicals were used as received.

Nanostructure Synthesis. *Solid-State Dewetting.* Supported Ag nanostructures were self-assembled on [0001]-oriented sapphire substrates using a solid-state dewetting procedure. Ultrathin films were sputter deposited to a thickness of 2.5 nm, after which they were placed in an alumina boat and loaded into a Lindberg Blue M tube furnace equipped with a quartz tube and the fittings needed to maintain an Ar gas flow of 100 sccm. The dewetting procedure utilized a heating regimen in which the temperature was

DOI: 10.1021/acscatal.8b02325
ACS Catal. 2018, 8, 8879−8888

elevated to 600 °C in 8 min, held there for 12 min, and then cooled to room temperature in 2 h.

Thin Film Deposition. The thin film depositions of Ag, Cu, Pd, Pt, and Au, which were used to obtain the results in Figure 7, were sputter deposited onto glass substrates at room temperature to a thickness of 10 nm. The depositions were carried out using a beam energy of 6 keV, penning ion gun currents of 200 μA, and an Ar pressure of 7×10^{-5} Torr. The base pressure of the sputter coater prior to deposition was less than 1×10^{-6} Torr.

Solution-Based Depositions. The solution-based depositions of Ag, which were used to obtain the results presented in Figure S3, were formed by reducing Ag^+ ions onto supported Ag seeds. The seeds were then placed into 1 mL of 10 mM ascorbic acid (95 °C), after which 3 mL of 1 mM $AgNO_3$ (95 °C) was added. After reaction times of 2, 5, or 8 min, the sample was removed, rinsed, and dried.

Galvanic Replacement Reactions. The AuAg nanoshells, which were used to obtain the results in Figure S4, were synthesized using substrate-based galvanic replacement reactions.[54] The 1 min reaction proceeded by placing dewetted Ag nanostructures into 3 mL of aqueous $HAuCl_4$ (10, 20, or 50 μM) heated to 95 °C after which the sample was removed, rinsed, and dried.

Spectroscopic Split Tests. Prior to the split test, the supported Ag catalyst was mounted to the motorized stage and the N_2 gas line was purged to remove any air that had accumulated. Stock solutions of 4-NP (60 μM) and $NaBH_4$ (6 mM) were then used to prepare a cuvette filled with 2 mL of reactants of the desired molarity (30 μM 4-NP, 3 mM $NaBH_4$) and dissolved oxygen concentration (<0.03, 1, or 7 mg·L^{-1}). The lowest dissolved oxygen concentration quoted (i.e., <0.03 mg·L^{-1}) represents the detection limit of the sensor (Vernier Optical DO Probe). Reducing the oxygen content to such low values requires exhaustive experimental procedures that are described in detail elsewhere.[31] The 1 and 7 mg·L^{-1} concentrations were obtained by allowing borohydride the time needed to scavenge enough dissolved oxygen to reduce the concentration from an ambient value of 8.3 mg·L^{-1} to the desired level. It should be noted that the loss of borohydride should not adversely influence the catalytic reduction of 4-NP since the molarity of borohydride exceeds that of dissolved oxygen by a factor of 96 and 13.7 for the 1 and 7 mg·L^{-1} concentrations, respectively. The time used was derived from a calibration curve that monitored the dissolved oxygen concentration as a function of time (Figure S8). Once the desired dissolved oxygen concentration was obtained, the spectrometer lid was closed and the supported catalyst was lowered into the reactants. Regardless of the dissolved oxygen concentration used, the reaction was carried out under N_2 to prevent the further uptake of O_2.

Other Catalysis Measurements. *Leaching Calibration Curves.* The calibration curve presented in Figure 4c was obtained by injecting 0.1 mL of aqueous $AgNO_3$ over a range of concentrations (1.2, 2, 4, 8, and 14 μM) into a cuvette containing a mixture of 1.9 mL of 4-NP (32 mM) and $NaBH_4$ (3.2 mM) with a dissolved oxygen concentration of 1 mg·L^{-1}. The time-dependent absorbance was then monitored from which k_{app} values were extracted. The calibration curve for the 7 mg·L^{-1} dissolved oxygen concentration (Figure 4e) was obtained in a similar manner, but where $AgNO_3$ concentrations of 1, 2, 5, 10, and 15 μM were used. These reactions, as well as the two listed below, were carried out under N_2 gas.

Oxidative Etching of Supported Ag Nanostructures. Six identical supported Ag nanostructure samples were placed in 1 mL of room temperature water with a dissolved oxygen concentration of 8.3 mg·L^{-1} for time intervals of 0.5, 2, 5, 10, 15, and 20 min. The samples were then removed, and the solutions were purged for 10 min with N_2 gas to remove the dissolved oxygen. The solutions were then poured into a cuvette containing 1 mL of N_2-purged 4-NP (60 μM) and $NaBH_4$ (6 mM), and the reaction was monitored. Figure 6b was derived from the data collected.

Oxidative Etching of Noble Metals in Saline Solutions. Films of Ag, Cu, Pd, Pt, and Au were placed into 1 mL of aqueous solutions with a dissolved oxygen concentration of 8.3 mg·L^{-1} and an identical solution into which 15 μM NaCl was added. After a 10 min interval, the film was removed and the solution was purged with N_2 gas. The reduction of 4-NP was then carried out as described in the previous example. Figure 7 was derived from the data collected.

ICP−OES. The reaction products derived from experiments identical to those shown in Figure 2b,c were analyzed for Ag. The test tubes used in the ICP−OES analysis were three times acid washed with 1% HNO_3 and 5 times rinsed with DI water. Ag analysis was conducted on acidified samples (5% *aqua regia*). Samples were diluted as needed to ensure accurate analysis, and internal standards were employed to account for matrix effects.

TEM Sample Preparation. The TEM work on the unsupported catalysts (Figures 5 and S6) was carried out on samples prepared by first dipping supported Ag nanostructures into aqueous 4-nitrophenol (30 μM) and borohydride (3 mM) with a dissolved oxygen concentration of 1 mg·L^{-1}. The supported structures were removed after 15 min, and the reaction was allowed to go to completion. Three drops of the product were then successively dropcast onto a Si_3N_4 TEM grid (total volume ≈ 21 μL).

Instrumentation. A Jasco V−730 spectrophotometer was used to monitor the catalytic reduction of 4-NP and to obtain the optical spectra of the supported Ag nanostructures. SEM images were acquired using a Magellan 400 (FEI) scanning electron microscope operating in secondary electron mode with a beam energy of 10 keV. TEM images were obtained using a FEI Titan 80-300 TEM. ICP−OES measurements were carried out using a PerkinElmer Optima 8000 Inductively Coupled Plasma Optically Emitting Spectra.

Simulations. The DDA simulations presented in Figure 3 were carried out using the DDSCAT (Version 7.3) software package.[55] The simulated structures were created using LAMMPS[56] and visualized using Visual Molecular Dynamics (VMD).[57] The nanostructure diameter of 33 nm was chosen to match the average value that was experimentally obtained (see Figure S2). The modeled structure was a truncated sphere where the degree of truncation was adjusted to obtain the experimental LSPR peak position. It is noted that the full width at half-maximum of the experimental LSPR peak is about a factor of 2 greater than the simulated peak because the self-assembly of nanostructures through solid-state dewetting results in a distribution of diameters where each has a different LSPR. The simulated Ag nanostructure and its sapphire support were defined by a total of 77 585 dipoles where the dielectric constants for Ag and sapphire were obtained from well-accepted sources.[58,59] The incident light was unpolarized with its k-vector normal to the substrate surface. The monolayer thickness was set to the distance between hexagonal

DOI: 10.1021/acscatal.8b02325
ACS Catal. 2018, 8, 8879−8888

close packed planes in the face centered cubic crystal structure of Ag (i.e., ML = $a/\sqrt{3}$ = 2.355 Å where "a" is the lattice constant) where the removal of a monolayer resulted in twice this thickness being removed from the diameter.

■ ASSOCIATED CONTENT

Supporting Information

The Supporting Information is available free of charge on the ACS Publications website at DOI: 10.1021/acscatal.8b02325.

Additional information including (i) details of the retrofit carried out on the Jasco V−730 spectrophotometer, (ii) the morphological characterization of the supported Ag nanostructures, (iii) split tests performed on Ag and AuAg nanostructures formed in solution, (iv) measurements showing that leached Ag nanostructures are catalytically inactive, (v) TEM images of unsupported Ag nanostructures, and (vi) the calibration curves used to obtain the results shown in Figures 2b−c and 6b (PDF)

■ AUTHOR INFORMATION

Corresponding Author

*E-mail: sneretina@nd.edu.

ORCID

Svetlana Neretina: 0000-0002-6889-4384

Author Contributions

§E.M. and R.A.H. contributed equally.

Notes

The authors declare no competing financial interest.

■ ACKNOWLEDGMENTS

This work was supported by a National Science Foundation Award (DMR-1707593) to S.N. The authors have benefited from the facilities available through the Notre Dame Integrated Imaging Facility (NDIIF). ICP−OES was conducted at the Center for Environmental Science and Technology (CEST) at the University of Notre Dame. The authors wish to acknowledge the technical expertise provided by J. Loftus in carrying out the ICP measurements and L. Hluchota and G. Brownell in the construction of the motorized stage.

■ REFERENCES

(1) Eremin, D. B.; Ananikov, V. P. Understanding Active Species in Catalytic Transformations: From Molecular Catalysis to Nanoparticles, Leaching, "Cocktails" of Catalysts and Dynamic Systems. *Coord. Chem. Rev.* **2017**, *346*, 2−19.

(2) Prieto, G.; Tüysüz, H.; Duyckaerts, N.; Knossalla, J.; Wang, G.-H.; Schüth, F. Hollow Nano- and Microstructures as Catalysts. *Chem. Rev.* **2016**, *116*, 14056−14119.

(3) Pachón, L. D.; Rothenberg, G. Transition-Metal Nanoparticles: Synthesis, Stability and the Leaching Issue. *Appl. Organomet. Chem.* **2008**, *22*, 288−299.

(4) Phan, N. T. S.; Van Der Sluys, M.; Jones, C. W. On the Nature of the Active Species in Palladium Catalyzed Mizoroki−Heck and Suzuki−Miyaura Couplings − Homogeneous or Heterogeneous Catalysis, A Critical Review. *Adv. Synth. Catal.* **2006**, *348*, 609−679.

(5) Zhang, Q.; Blom, D. A.; Wang, H. Nanoporosity-Enhanced Catalysis on Subwavelength Au Nanoparticles: a Plasmon-Enhanced Spectroscopic Study. *Chem. Mater.* **2014**, *26*, 5131−5142.

(6) Rossy, C.; Majimel, J.; Fouquet, E.; Delacôte, C.; Boujtita, M.; Labrugère, C.; Tréguer-Delapierre, M.; Felpin, F.-X. Stabilisation of Carbon-Supported Palladium Nanoparticles through the Formation of an Alloy with Gold: Application to the Sonogashira Reaction. *Chem. - Eur. J.* **2013**, *19*, 14024−14029.

(7) Zhang, N.; Xu, Y.-J. Aggregation- and Leaching-Resistant, Reusable, and Multifunctional Pd@CeO_2 as a Robust Nanocatalyst Achieved by a Hollow Core−Shell Strategy. *Chem. Mater.* **2013**, *25*, 1979−1988.

(8) Galeandro-Diamant, T.; Sayah, R.; Zanota, M.-L.; Marrot, S.; Veyre, L.; Thieuleux, C.; Meille, V. Pt Nanoparticles Immobilized in Mesostructured Silica: A Non-Leaching Catalyst for 1-Octene Hydrosilylation. *Chem. Commun.* **2017**, *53*, 2962−2965.

(9) Lee, J.; Kim, S. M.; Lee, I. S. Functionalization of Hollow Nanoparticles for Nanoreactor Applications. *Nano Today* **2014**, *9*, 631−667.

(10) Roa, R.; Angioletti-Uberti, S.; Lu, Y.; Dzubiella, J.; Piazza, F.; Ballauff, M. Catalysis by Metallic Nanoparticles in Solution: Thermosensitive Microgels as Nanoreactors. *Z. Phys. Chem.* **2018**, *232*, 773−803.

(11) Astruc, D. Palladium Nanoparticles as Efficient Green Homogeneous and Heterogeneous Carbon−Carbon Coupling Precatalysts: A Unifying View. *Inorg. Chem.* **2007**, *46*, 1884−1894.

(12) Weck, M.; Jones, C. W. Mizoroki-Heck Coupling Using Immobilized Molecular Precatalysts: Leaching Active Species from Pd Pincers, Entrapped Pd Salts, and Pd NHC Complexes. *Inorg. Chem.* **2007**, *46*, 1865−1875.

(13) Kashin, A. S.; Ananikov, V. P. Catalytic C−C and C−Heteroatom Bond Formation Reactions: In Situ Generated or Preformed Catalysts? Complicated Mechanistic Picture Behind Well-Known Experimental Procedures. *J. Org. Chem.* **2013**, *78*, 11117−11125.

(14) Köhler, K.; Heidenreich, R. G.; Krauter, J. G. E.; Pietsch, J. Highly Active Palladium/Activated Carbon Catalysts for Heck Reactions: Correlation of Activity, Catalyst Properties, and Pd Leaching. *Chem. - Eur. J.* **2002**, *8*, 622−631.

(15) de Vries, J. G. A Unifying Mechanism for All High-Temperature Heck Reactions. The Role of Palladium Colloids and Anionic Species. *Dalton Trans.* **2006**, 421−429.

(16) Cassol, C. C.; Umpierre, A. P.; Machado, G.; Wolke, S. I.; Dupont, J. The Role of Pd Nanoparticles in Ionic Liquid in the Heck Reaction. *J. Am. Chem. Soc.* **2005**, *127*, 3298−3299.

(17) Nigra, M. M.; Ha, J.-M.; Katz, A. Identification of Site Requirements for Reduction of 4-Nitrophenol using Gold Nanoparticle Catalysts. *Catal. Sci. Technol.* **2013**, *3*, 2976−2983.

(18) Collins, G.; Holmes, J. D. Engineering Metallic Nanoparticles for Enhancing and Probing Catalytic Reactions. *Adv. Mater.* **2016**, *28*, 5689−5695.

(19) Briggs, B. D.; Bedford, N. M.; Seifert, S.; Koerner, H.; Ramezani-Dakhel, H.; Heinz, H.; Naik, R. R.; Frenkel, A. I.; Knecht, M. R. Atomic-Scale Identification of Pd Leaching in Nanoparticle Catalyzed C−C coupling: Effects of Particle Surface Disorder. *Chem. Sci.* **2015**, *6*, 6413−6419.

(20) Mahmoud, M. A.; Garlyyev, B.; El-Sayed, M. A. Determining the Mechanism of Solution Metallic Nanocatalysis with Solid and Hollow Nanoparticles: Homogeneous or Heterogeneous. *J. Phys. Chem. C* **2013**, *117*, 21886−21893.

(21) Taladriz-Blanco, P.; Hervés, P.; Pérez-Juste, J. Supported Pd Nanoparticles for Carbon−Carbon Coupling Reactions. *Top. Catal.* **2013**, *56*, 1154−1170.

(22) Pérez-Lorenzo, M. Palladium Nanoparticles as Efficient Catalysts for Suzuki Cross-Coupling Reactions. *J. Phys. Chem. Lett.* **2012**, *3*, 167−174.

(23) Thathagar, M. B.; ten Elshof, J. E.; Rothenberg, G. Pd Nanoclusters in C−C Coupling Reactions: Proof of Leaching. *Angew. Chem., Int. Ed.* **2006**, *45*, 2886−2890.

(24) Zhao, P.; Feng, X.; Huang, D.; Yang, G.; Astruc, D. Basic Concepts and Recent Advances in Nitrophenol Reduction by Gold- and Other Transition Metal Nanoparticles. *Coord. Chem. Rev.* **2015**, *287*, 114−136.

DOI: 10.1021/acscatal.8b02325
ACS Catal. 2018, 8, 8879−8888

(25) Aditya, T.; Pal, A.; Pal, T. Nitroarene Reduction: A Trusted Model Reaction to Test Nanoparticle Catalysts. *Chem. Commun.* **2015**, *51*, 9410−9431.
(26) Hervés, P.; Pérez-Lorenzo, M.; Liz-Marzán, L. M.; Dzubiella, J.; Lu, Y.; Ballauff, M. Catalysis by Metallic Nanoparticles in Aqueous Solution: Model Reactions. *Chem. Soc. Rev.* **2012**, *41*, 5577−5587.
(27) Gu, S.; Wunder, S.; Lu, Y.; Ballauff, M.; Fenger, R.; Rademann, K.; Jaquet, B. Kinetic Analysis of the Catalytic Reduction of 4-Nitrophenol by Metallic Nanoparticles. *J. Phys. Chem. C* **2014**, *118*, 18618−18625.
(28) Saha, S.; Pal, A.; Kundu, S.; Basu, S.; Pal, T. Photochemical Green Synthesis of Calcium-Alginate-Stabilized Ag and Au Nanoparticles and Their Catalytic Application to 4-Nitrophenol Reduction. *Langmuir* **2010**, *26*, 2885−2893.
(29) Menumerov, E.; Gilroy, K. D.; Hajfathalian, M.; Murphy, C. J.; McKenzie, E. R.; Hughes, R. A.; Neretina, S. Plastically Deformed Cu-Based Alloys as High-Performance Catalysts for the Reduction of 4-Nitrophenol. *Catal. Sci. Technol.* **2016**, *6*, 5737−5745.
(30) Menumerov, E.; Hughes, R. A.; Neretina, S. One-Step Catalytic Reduction of 4-Nitrophenol through the Direct Injection of Metal Salts into Oxygen-Depleted Reactants. *Catal. Sci. Technol.* **2017**, *7*, 1460−1464.
(31) Menumerov, E.; Hughes, R. A.; Neretina, S. Catalytic Reduction of 4-Nitrophenol: A Quantitative Assessment of the Role of Dissolved Oxygen in Determining the Induction Time. *Nano Lett.* **2016**, *16*, 7791−7797.
(32) Zheng, G.; Polavarapu, L.; Liz-Marzán, L. M.; Pastoriza-Santos, I.; Pérez-Juste, J. Gold Nanoparticle-Loaded Filter Paper: A Recyclable Dip-Catalyst for Real-Time Monitoring by Surface Enhanced Raman Scattering. *Chem. Commun.* **2015**, *51*, 4572−4575.
(33) Hariprasad, E.; Radhakrishnan, T. P. A Highly Efficient and Extensively Reusable "Dip Catalyst" Based on a Silver-Nanoparticle-Embedded Polymer Thin Film. *Chem. - Eur. J.* **2010**, *16*, 14378−14384.
(34) Hajfathalian, M.; Gilroy, K. D.; Yaghoubzade, A.; Sundar, A.; Tan, T.; Hughes, R. A.; Neretina, S. Photocatalytic Enhancements to the Reduction of 4-Nitrophenol by Resonantly Excited Triangular Gold−Copper Nanostructures. *J. Phys. Chem. C* **2015**, *119*, 17308−17315.
(35) Thompson, C. V. Solid-State Dewetting of Thin Films. *Annu. Rev. Mater. Res.* **2012**, *42*, 399−434.
(36) Long, R.; Zhou, S.; Wiley, B. J.; Xiong, Y. Oxidative Etching for Controlled Synthesis of Metal Nanocrystals: Atomic Addition and Subtraction. *Chem. Soc. Rev.* **2014**, *43*, 6288−6310.
(37) Zheng, Y.; Zeng, J.; Ruditskiy, A.; Liu, M.; Xia, Y. Oxidative Etching and Its Role in Manipulating the Nucleation and Growth of Noble-Metal Nanocrystals. *Chem. Mater.* **2014**, *26*, 22−33.
(38) Draine, B. T.; Flatau, P. J. Discrete-Dipole Approximation For Scattering Calculations. *J. Opt. Soc. Am. A* **1994**, *11*, 1491−1499.
(39) Deraedt, C.; Salmon, L.; Gatard, S.; Ciganda, R.; Hernandez, R.; Ruiz, J.; Astruc, D. Sodium Borohydride Stabilizes Very Active Gold Nanoparticle Catalysts. *Chem. Commun.* **2014**, *50*, 14194−14196.
(40) Pradhan, N.; Pal, A.; Pal, T. Silver Nanoparticle Catalyzed Reduction of Aromatic Nitro Compounds. *Colloids Surf., A* **2002**, *196*, 247−257.
(41) Im, S. H.; Lee, Y. T.; Wiley, B.; Xia, Y. Large-Scale Synthesis of Silver Nanocubes: The Role of HCl in Promoting Cube Perfection and Monodispersity. *Angew. Chem.* **2005**, *117*, 2192−2195.
(42) Xiong, Y.; Chen, J.; Wiley, B.; Xia, Y.; Aloni, S.; Yin, Y. Understanding the Role of Oxidative Etching in the Polyol Synthesis of Pd Nanoparticles with Uniform Shape and Size. *J. Am. Chem. Soc.* **2005**, *127*, 7332−7333.
(43) Jin, M.; He, G.; Zhang, H.; Zeng, J.; Xie, Z.; Xia, Y. Shape-Controlled Synthesis of Copper Nanocrystals in an Aqueous Solution with Glucose as a Reducing Agent and Hexadecylamine as a Capping Agent. *Angew. Chem., Int. Ed.* **2011**, *50*, 10560−10564.
(44) Langille, M. R.; Personick, M. L.; Mirkin, C. A. Plasmon-Mediated Syntheses of Metallic Nanostructures. *Angew. Chem., Int. Ed.* **2013**, *52*, 13910−13940.
(45) Zhang, Q.; Yang, Y.; Li, J.; Iurilli, R.; Xie, S.; Qin, D. Citrate-Free Synthesis of Silver Nanoplates and the Mechanistic Study. *ACS Appl. Mater. Interfaces* **2013**, *5*, 6333−6345.
(46) Garrett, C. E.; Prasad, K. The Art of Meeting Palladium Specifications in Active Pharmaceutical Ingredients Produced by Pd-Catalyzed Reactions. *Adv. Synth. Catal.* **2004**, *346*, 889−900.
(47) Cho, D.-G.; Sessler, J. L. Modern Reaction-Based Indicator Systems. *Chem. Soc. Rev.* **2009**, *38*, 1647−1662.
(48) Levard, C.; Hotze, E. M.; Lowry, G. V.; Brown, Jr. G. E. Environmental Transformations of Silver Nanoparticles: Impact on Stability and Toxicity. *Environ. Sci. Technol.* **2012**, *46*, 6900−6914.
(49) Zhang, W.; Xiao, B.; Fang, T. Chemical Transformation of Silver Nanoparticles in Aquatic Environments: Mechanism, Morphology and Toxicity. *Chemosphere* **2018**, *191*, 324−334.
(50) Xiu, Z.-M.; Zhang, Q.-B.; Puppala, H. L.; Colvin, V. L.; Alvarez, P. J. J. Negligible Particle-Specific Antibacterial Activity of Silver Nanoparticles. *Nano Lett.* **2012**, *12*, 4271−4275.
(51) Ivask, A.; ElBadawy, A.; Kaweeteerawat, C.; Boren, D.; Fischer, H.; Ji, Z.; Chang, C. H.; Liu, R.; Tolaymat, T.; Telesca, D.; Zink, J. I.; Cohen, Y.; Holden, P. A.; Godwin, H. A. Toxicity Mechanisms in Escherichia *coli* Vary for Silver Nanoparticles and Differ from Ionic Silver. *ACS Nano* **2014**, *8*, 374−386.
(52) Loza, K.; Diendorf, J.; Sengstock, C.; Ruiz-Gonzalez, L.; Gonzalez-Calbet, J. M.; Vallet-Regi, M.; Köller, M.; Epple, M. The Dissolution and Biological Effects of Silver Nanoparticles in Biological Media. *J. Mater. Chem. B* **2014**, *2*, 1634−1643.
(53) Johnston, K. A.; Stabryla, L. M.; Smith, A. M.; Gan, X. Y.; Gilbertson, L. M.; Millstone, J. E. Impacts of Broth Chemistry on Silver Ion Release, Surface Chemistry Composition, and Bacterial Cytotoxicity of Silver Nanoparticles. *Environ. Sci.: Nano* **2018**, *5*, 304−312.
(54) Gilroy, K. D.; Farzinpour, P.; Sundar, A.; Tan, T.; Hughes, R. A.; Neretina, S. Substrate-Based Galvanic Replacement Reactions Carried out on Heteroepitaxially Formed Silver Templates. *Nano Res.* **2013**, *6*, 418−428.
(55) Draine, B. T.; Flatau, P. J. User Guide to the Discrete Dipole Approximation Code DDSCAT 7.2. 2012, arXiv:1202.3424. arXiv.org e-Print archive. http://arXiv.org/abs/1202.3424 (accessed January 2018).
(56) Plimpton, S. Fast Parallel Algorithms for Short-Range Molecular Dynamics. *J. Comput. Phys.* **1995**, *117*, 1−19.
(57) Humphrey, W.; Dalke, A.; Schulten, K. VMD: Visual Molecular Dynamics. *J. Mol. Graphics* **1996**, *14*, 33−38.
(58) Palik, E. D. *Handbook of Optical Constants of Solids*; Academic Press: New York, NY, 1998.
(59) Johnson, P. B.; Christy, R. W. Optical Constants of the Noble Metals. *Phys. Rev. B* **1972**, *6*, 4370−4379.

DOI: 10.1021/acscatal.8b02325
ACS Catal. 2018, 8, 8879−8888